Reactions of Methyl Fluoride with Atomic Transition-Metal and Main-Group Cations: Gas-Phase Room-Temperature Kinetics and Periodicities in Reactivity

Xiang Zhao, Gregory K. Koyanagi, and Diethard K. Bohme*

Centre for Research in Mass Spectrometry and Centre for Research in Earth and Space Science, Department of Chemistry, York University, Toronto, Ontario, Canada M3J 1P3

Received: April 28, 2006; In Final Form: July 14, 2006

Reactions of CH_3F have been surveyed systematically at room temperature with 46 different atomic cations using an inductively coupled plasma/selected-ion flow tube tandem mass spectrometer. Rate coefficients and product distributions were measured for the reactions of fourth-period atomic ions from K^+ to Se^+, of fifth-period atomic ions from Rb^+ to Te^+ (excluding Tc^+), and of sixth-period atomic ions from Cs^+ to Bi^+. Primary reaction channels were observed corresponding to F atom transfer, CH_3F addition, HF elimination, and H_2 elimination. The early-transition-metal cations exhibit a much more active chemistry than the late-transition-metal cations, and there are periodic features in the chemical activity and reaction efficiency that maximize with Ti^+, As^+, Y^+, Hf^+, and Pt^+. F atom transfer appears to be thermodynamically controlled, although a periodic variation in efficiency is observed within the early-transition-metal cations which maximizes with Ti^+, Y^+, and Hf^+. Addition of CH_3F was observed exclusively (>99%) with the late-fourth-period cations from Mn^+ to Ga^+, the fifth-period cations from Ru^+ to Te^+, and the sixth-period cations from Hg^+ to Bi^+ as well as Re^+. Periodic trends are observed in the effective bimolecular rate coefficient for CH_3F addition, and these are consistent with expected trends in the electrostatic binding energies of the adduct ions and measured trends in the standard free energy of addition. HF elimination is the major reaction channel with As^+, while dehydrogenation dominates the reactions of W^+, Os^+, Ir^+, and Pt^+. Sequential F atom transfer is observed with the early-transition-metal cations, with the number of F atoms transferred increasing across the periodic table from two to four, maximizing at four for the group 5 cations $Nb^+(d^4)$ and $Ta^+(d^3s^1)$, and stopping at two with $V^+(d^4)$. Sequential CH_3F addition was observed with many atomic cations and all of the metal mono- and multifluoride cations that were formed.

Introduction

Methyl fluoride is a simple model molecule well suited for studies of C−F bond activation and the competition between C−F and C−H activation. Although selective activation of C−F bonds has been the subject of a recent feature article by Mazurek and Schwarz with a particular view to surface and gas-phase reactions,[1] experimental studies of C−F bond activation by atomic cations have not been extensive, particularly with CH_3F. FT-ICR mass spectrometry, in which laser ablation/ionization serves as the source of atomic cations, has been used previously to study F atom transfer from CH_3F to Ti^+,[2] from CH_3F to Ca^+, Sc^+, Ti^+, V^+, and Y^+,[3] and from CF_4, CHF_3, CH_3F, C_2F_6, 1,1-$C_2H_4F_2$, and C_6F_6 to six lanthanide monocations, Ce^+, Pr^+, Sm^+, Ho^+, Tm^+, and Yb^+.[4] Only one theoretical investigation appears to have been published so far, that of Harvey et al.,[3] which points toward a "harpoon mechanism" for the F atom transfer from CH_3F to Ca^+.

The recent configuration of an inductively coupled plasma/selected-ion flow tube (ICP/SIFT) tandem mass spectrometer in our laboratory has provided the means to survey trends in chemical kinetics for room-temperature reactions of atomic cations with gaseous molecules across and down the periodic table. Already we have surveyed reactions of atomic cations in the fourth, fifth, and sixth periods with molecular oxygen, both in the absence[5] and in the presence[6] of benzene, with hexafluorobenzene,[7,8] with benzene,[9] with nitrous oxide,[10] with carbon dioxide,[11] and with carbon disulfide.[12] These surveys are driven in part by their fundamental importance, but also by the use of molecules for the chemical resolution of isobaric interferences in ICP mass spectrometry.[13,14] Here we report results obtained for reactions of 46 different atomic cations with methyl fluoride. Methyl fluoride has been used recently as a selective reagent in the resolution of the $^{87}Rb^+/^{87}Sr^+$ isobaric interference in the dynamic reaction cell of an ICP-MS instrument used for the Rb/Sr age determination of magnetic rocks.[15] We have systematically surveyed reactions of CH_3F with fourth-period atomic cations from K^+ to Se^+, of fifth-period atomic cations from Rb^+ to Te^+ (excluding Tc^+), and of sixth-period atomic cations from Cs^+ to Bi^+. The results of our recent ICP/SIFT measurements of room-temperature reactions of 14 atomic lanthanide cations with methyl fluoride already have appeared in the literature.[16]

Experimental Method

The experimental results reported here were obtained using the SIFT tandem mass spectrometer described in detail elsewhere.[13,14] This instrument was recently modified to accept ions generated in an inductively coupled plasma (ICP) torch (ELAN series, Perkin-Elmer SCIEX) through an atmosphere/vacuum interface. The ICP ion source and interface also have been described previously,[17,18] as has the preparation of the solutions

* To whom correspondence should be addressed. E-mail: dkbohme@yorku.ca. Phone: (416) 736-2100, ext 66188. Fax: (416) 736-5936.

10.1021/jp062625a CCC: $33.50
Published on Web 08/18/2006

TABLE 1: Rate Coefficients (cm^3 $molecule^{-1}$ s^{-1}), Reaction Efficiencies (k/k_c), and Product Distributions (PDs) for Reactions of Atomic Ions M^+ with Methyl Fluoride in Helium at 0.35 ± 0.01 Torr and 295 ± 2 K Ordered According to the Period in the Periodic Table[a]

M^+	k[b]	k_{cap}[c]/10^{-9}	k/k_c	primary product	PD[d]	higher order product ions
K^+	$<1 \times 10^{-12}$	2.27	$<4 \times 10^{-4}$	none		
Ca^+	2.6×10^{-10}	2.26	0.12	CaF^+	100	$CaF^+(CH_3F)_{1-2}$
Sc^+	1.1×10^{-9}	2.21	0.50	ScF^+	100	$ScF_2^+(CH_3F)_{0-4}$
Ti^+	1.3×10^{-9}	2.19	0.59	TiF^+	100	$TiF_{2,3}^+$, $TiF_2^+(CH_3F)_{1-4}$, $TiF_3^+(CH_3F)_{1-3}$, CH_2F^+, CH_3^+, $CH_3^+(CH_3F)$, $CH_2F^+(CH_3F)$
V^+	1.7×10^{-10}	2.15	0.079	VF^+	100	$VF^+(CH_3F)_{1-5}$, $VF_2^+(CH_3F)_{0-4}$
Cr^+	1.1×10^{-11}	2.13	5.3×10^{-3}	Cr^+CH_3F	98	$Cr^+(CH_3F)_{2-4}$
				CH_2F^+	2	
Mn^+	6.0×10^{-12}	2.12	2.8×10^{-3}	Mn^+CH_3F	100	$Mn^+(CH_3F)_2$
Fe^+	1.5×10^{-11}	2.10	7.1×10^{-3}	Fe^+CH_3F	100	$Fe^+(CH_3F)_4$
Co^+	1.8×10^{-11}	2.10	8.6×10^{-3}	Co^+CH_3F	100	$Co^+(CH_3F)_{2-4}$
Ni^+	2.3×10^{-11}	2.09	0.011	Ni^+CH_3F	100	$Ni^+(CH_3F)_{2-4}$
Cu^+	8.7×10^{-12}	2.08	4.2×10^{-3}	Cu^+CH_3F	100	$Cu^+(CH_3F)_2$
Zn^+	4.6×10^{-12}	2.08	2.2×10^{-3}	Zn^+CH_3F	100	$Zn^+(CH_3F)_2$
Ga^+	$\leq 5.0 \times 10^{-13}$	2.05	$\leq 2.4 \times 10^{-4}$	Ga^+CH_3F	100	$Ga^+(CH_3F)_2$
Ge^+	5.8×10^{-10}	2.03	0.29	GeF^+	100	$GeF^+(CH_3F)_{1,2}$
As^+	9.1×10^{-10}	2.01	0.45	$AsCH_2^+$	97	$AsCH_2^+(CH_3F)$
				As^+CH_3F	3	
Se^+	$<1 \times 10^{-13}$	2.00	$<5 \times 10^{-4}$	none		
Rb^+	1.3×10^{-12}	1.97	6.7×10^{-4}	Rb^+CH_3F	100	none
Sr^+	1.4×10^{-11}	1.97	7.1×10^{-3}	SrF^+	96	$SrF^+(CH_3F)_{1,2}$
				Sr^+CH_3F	4	$Sr^+(CH_3F)_2$
Y^+	1.7×10^{-9}	1.96	0.86	YF^+	100	$YF_2^+(CH_3F)_{0-4}$
Zr^+	1.2×10^{-9}	1.95	0.60	ZrF^+	100	$ZrF_{2,3}^+$, $ZrF_3^+(CH_3F)_{1-3}$, CH_3^+, $CH_3^+(CH_3F)$
Nb^+	7.4×10^{-10}	1.95	0.38	NbF^+	100	NbF_{2-4}^+, $NbF_4^+(CH_3F)_{1,2}$
Mo^+	2.8×10^{-12}	1.94	1.4×10^{-3}	Mo^+CH_3F	100	$Mo^+(CH_3F)_{2-4}$
Ru^+	3.2×10^{-12}	1.94	1.6×10^{-3}	Ru^+CH_3F	100	$Ru^+(CH_3F)_{2,3}$
Rh^+	2.7×10^{-12}	1.91	1.4×10^{-3}	Rh^+CH_3F	100	$Rh^+(CH_3F)_{2,3}$
Pd^+	5.1×10^{-12}	1.91	2.7×10^{-3}	Pd^+CH_3F	100	$Pd^+(CH_3F)_{2,3}$
Ag^+	3.1×10^{-12}	1.90	1.6×10^{-3}	Ag^+CH_3F	100	$Ag^+(CH_3F)_{2,3}$
Cd^+	1.4×10^{-12}	1.89	7.4×10^{-4}	Cd^+CH_3F	100	$Cd^+(CH_3F)_2$
In^+	1.2×10^{-12}	1.88	6.4×10^{-4}	In^+CH_3F	100	none
Sn^+	1.9×10^{-12}	1.88	1.0×10^{-3}	Sn^+CH_3F	100	$Sn^+(CH_3F)_2$
Sb^+	4.7×10^{-12}	1.88	2.5×10^{-3}	Sb^+CH_3F	100	$Sb^+(CH_3F)_2$
Te^+	5.6×10^{-13}	1.87	3.0×10^{-4}	Te^+CH_3F	100	none
Cs^+	$\leq 5.0 \times 10^{-13}$	1.87	$\leq 2.8 \times 10^{-4}$	Cs^+CH_3F	100	none
Ba^+	6.4×10^{-11}	1.86	0.034	BaF^+	100	$BaF^+(CH_3F)_{1-3}$
La^+	4.5×10^{-10}	1.86	0.24	LaF^+	100	LaF_2^+, $LaF_2^+(CH_3F)_{1-3}$
Hf^+	1.1×10^{-9}	1.82	0.62	HfF^+	100	HfF_{2-3}^+, $HfF_3^+(CH_3F)_{1,2}$, CH_3^+, $CH_3^+(CH_3F)$, CH_2F^+, $CH_2F^+(CH_3F)$
Ta^+	7.0×10^{-10}	1.82	0.38	TaF^+	100	TaF_{2-4}^+, $TaF_{3,4}^+(CH_3F)_{1,2}$
W^+	1.9×10^{-10}	1.82	0.10	$WCHF^+$	95	$W(CHF)_2^+(CH_3F)_{0-2}$
				W^+CH_3F	5	$W^+(CH_3F)_2$
Re^+	1.7×10^{-12}	1.82	9.3×10^{-4}	Re^+CH_3F	100	$Re^+(CH_3F)_{2,3}$
Os^+	1.8×10^{-10}	1.82	0.099	$OsCHF^+$	98	$OsCHF^+(CH_3F)_{1,2}$
				$OsCH_2^+$	2	$Os^+(CH_2)(CHF)_{0,1}(CH_3F)_{1,2}$
Ir^+	6.6×10^{-10}	1.82	0.36	$IrCHF^+$	97	$IrCHF^+(CH_3F)_{1-3}$, $Ir(CHF)_2^+(CH_3F)_{0-2}$, $Ir(CH_2)(CHF)_{1,2}^+(CH_3F)_{1,2}$, $Ir(CH_2)_2(CHF)^+(CH_3F)_{1,2}$
				$IrCH_2^+$	3	
Pt^+	1.4×10^{-9}	1.81	0.80	$PtCHF^+$	95	$PtCHF^+(CH_3F)_{2,3}$
				$PtCH_2^+$	5	$PtCH_2^+(CH_3F)_{1,2}$
Au^+	8.9×10^{-12}	1.80	4.9×10^{-3}	Au^+CH_3F	88	$Au^+(CH_3F)_2$
				$AuCH_2^+$	12	$AuCH_2^+(CH_3F)_{1,2}$
Hg	2.5×10^{-12}	1.80	1.4×10^{-3}	Hg^+CH_3F	100	$Hg^+(CH_3F)_2$
Tl^+	5.2×10^{-13}	1.80	2.9×10^{-4}	Tl^+CH_3F	100	none
Pb^+	$\leq 5.0 \times 10^{-13}$	1.80	$\leq 2.8 \times 10^{-4}$	Pb^+CH_3F	100	none
Bi^+	1.0×10^{-12}	1.80	5.8×10^{-4}	Bi^+CH_3F	100	none

[a] Higher order product ions are also indicated. [b] Measured reaction rate coefficient with an estimated accuracy of ±30%. The rate coefficient for an addition reaction is an effective bimolecular rate coefficient, $k = k_3[He]$, where k_3 is the rate coefficient for the corresponding termolecular reaction. This rate coefficient will depend on the helium pressure (and the nature of the stabilizing third body). [c] Calculated collision rate coefficient (see the text). [d] PD = product distribution expressed as a percentage with an estimated uncertainty of less than 5%. The minor products (≤5%) are not due to impurities given the nature of the known impurities (SiF_4 and $(CH_3)_2O$) and their amounts (≤1%).

containing the metal salt of interest which were peristaltically pumped via a nebulizer into the plasma.[11]

Atomic ions emerge from the ICP at a nominal ion temperature of 5500 K with corresponding Boltzmann state distributions. These distributions have been derived from available optical spectra[19,20] and reported by us previously for the two electronic spin states with the highest population at 5500 K.[10] Energy levels as high as 3.7 eV (3×10^4 cm^{-1}) were included in the calculations. The calculations show that excited states of the main-group elemental cations except Ba^+ are high in energy and contribute little (never more than 10%) to the total ion population at 5500 K. The ground ^2S state of Ba^+ contributes 44% and the excited ^2D state 55% at 5500 K. The state distributions are more variable for the transition-metal cations.

Excited states contribute 20% or less toward the populations of Cr^+, Mn^+, Ni^+, Cu^+, Zn^+, Rh^+, Pd^+, Ag^+, Cd^+ Re^+, Au^+, and Hg^+ and 50% or more toward the populations of Ti^+, Y^+, Zr^+, Nb^+, La^+, and Ir^+, with Sc^+, V^+, Fe^+, Co^+, Mo^+, Ru^+, Hf^+, Ta^+, W^+, and Pt^+ having intermediate distributions with Os^+ not known.

The ions emerging from the ICP are injected through a differentially pumped sampling interface into a quadrupole mass spectrometer and, after mass analysis, introduced through an aspirator-like interface into flowing helium carrier gas at 0.35 Torr and 295 ± 2 K. The ions are allowed to react with added CH_3F a few milliseconds downstream of the flow tube.

After extraction from the ICP, the plasma ions may experience both radiative electronic-state relaxation and collisional electronic-state relaxation. The latter may occur already with argon as the extracted plasma cools upon sampling and then by collisions with He atoms in the flow tube (ca. 4×10^5 collisions with He) prior to the reaction region, but the actual extent of electronic relaxation (either radiative or collisional) is not known and is difficult to assess. Almost all of the electronic states of the transition-metal ions have positive parity; electric dipole transitions between states of the same parity are forbidden (Laporte rule).[21] This means that radiative transitions between different states in metal cations can be achieved only by either magnetic dipole or electric quadrupole radiation. The probabilities for these transitions are very low, and the resulting radiative lifetimes are on the order of seconds or larger. The time interval in the ICP/SIFT experiments between the exit of the ICP source and the entrance in the reaction region is ca. 20 ms, and therefore, no major modification of state distributions can occur in this time interval by forbidden radiative decay. That having been said, there were no indications of excited-state effects in our previous measurements of reactions of N_2O with atomic cations derived from the same ICP source operated in the same manner, except with Pt^+.[10] The many collisions experienced by the atomic cations with the quite polarizable Ar atoms as they emerge from the ICP and the ca. 4×10^5 collisions with He atoms in the flow tube (the helium buffer gas pressure was 0.35 ± 0.01 Torr) appear to be sufficient to provide for the thermalization of the excited states and ensure that the atomic ions reach a translational temperature equal to the tube temperature of 295 ± 2 K prior to entering the reaction region. However, the exact extent of electronic relaxation is uncertain. Clues to the presence of excited electronic states of the atomic ions in the reaction region can be found in the product ions observed and the shape of the semilogarithmic decay of the reacting atomic ion upon addition of neutral reactant. Curvature will appear in the measured atomic ion decay when the ground state and excited state react at different rates even when they give the same product ions. An excited-state effect cannot be seen when the products and reaction rates are the same for both the ground and excited states, but in this case the measured atomic ion decay defines the ground-state kinetics. Our growing experience has shown that excited states can reveal themselves when the ground state of the atomic ion reacts only slowly by termolecular addition and excited states react rapidly in a bimolecular fashion. Our previous studies indicate that the collisions with Ar and He ensure that most atomic ions reach a translational and internal temperature equal to the tube temperature of 295 ± 2 K prior to entering the reaction region.[5−12]

Reactant and product ions were sampled still further downstream with a second quadrupole mass spectrometer and were measured as a function of added reactant. The resulting profiles provide information about product ion distributions, reaction rate coefficients, and reaction molecularity. Rate coefficients for the primary bimolecular ion−molecule reactions are determined from the rate of decay of the reactant ion intensity with an uncertainty estimated to be less than ±30%.[13,14] Often slow adduct formation is observed exclusively, and this can introduce curvature into the primary ion decay due to the occurrence of the reverse reaction (the extent of curvature will depend on the strength of the adduct bond being formed). Weak adduct bonding can lead to early curvature in the ion decay and so prevent the proper definition of the forward rate coefficient; only the determination of a lower limit to the rate coefficient is possible under such conditions. The approach to equilibrium can be monitored with a plot of the ratio of the concentration of the adduct ion over that of the bare ion against the flow of the added reactant. This ratio will curve upward as equilibrium is approached and increase linearly with flow when equilibrium is achieved. Linearity in the ratio plot provides a measure of the equilibrium constant, K, and so the standard free energy change, $\Delta G°_T$, for the addition reaction since $\Delta G°_T = -RT \ln K$.

Methyl fluoride was introduced into the reaction region of the SIFT as a dilute mixture in helium (∼15%). The methyl fluoride was obtained commercially and was of high purity (Matheson Gas Products, >99%), with SiF_4 and $(CH_3)_2O$ being the quoted impurities.

Results and Discussion

The reactions of CH_3F were measured with 46 atomic cations, including 29 transition-metal and 17 main-group cations. Both the primary and higher order chemistries were monitored. Table 1 summarizes the measured rate coefficients, reaction efficiencies, observed primary products and product distributions, and observed higher order product ions. The reaction efficiency is taken to be equal to the ratio k/k_c, where k is the experimentally measured rate coefficient and k_c is the capture or collision rate coefficient. k_c was computed using the algorithm of the modified variational transition-state/classical trajectory theory developed by Su and Chesnavich[22] with a polarizability $\alpha(CH_3F) = 2.97$ Å^3,[23] and a permanent dipole moment $\mu_D(CH_3F) = 1.85$ D.[24]

The primary reactions exhibit a wide range in reactivity with measured rate coefficients in the range from $<10^{-13}$ to 1.5×10^{-9} cm^3 molecule^{-1} s^{-1}. The five different channels indicated in reaction 1

$$M^+ + CH_3F \rightarrow M^+CH_3F \quad (1a)$$

$$\rightarrow MF^+ + CH_3 \quad (1b)$$

$$\rightarrow MCH_2^+ + HF \quad (1c)$$

$$\rightarrow MCHF^+ + H_2 \quad (1d)$$

$$\rightarrow CH_2F^+ + MH \quad (1e)$$

were observed in varying amounts with different atomic ions. Channel 1a corresponds to molecular addition. The CH_3F addition is assumed to occur in a termolecular fashion under our experimental conditions, with He acting as the third body; no attempt was made to measure the pressure dependence of this channel since a large range in pressure was not experimentally accessible. The bimolecular channels correspond to F atom transfer, channel 1b, HF elimination, channel 1c, dehydrogenation, channel 1d, and hydride transfer to form the neutral metal hydride, channel 1e. No other bimolecular channels were observed. Electron transfer is endothermic for all the atomic

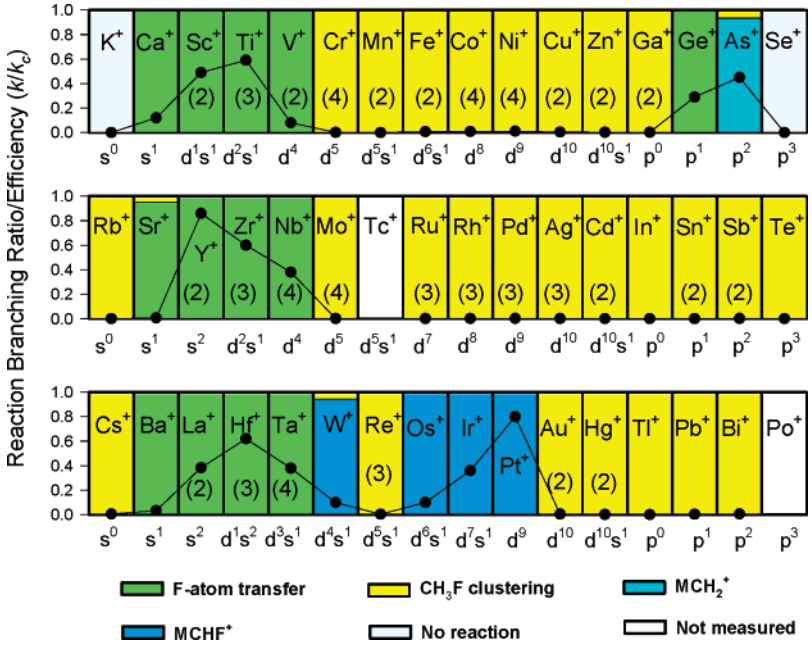

Figure 1. Periodic variations observed in the efficiencies, k/k_c (represented as solid circles), for reactions of atomic cations with methyl fluoride. k represents the measured reaction rate coefficient, and k_c is the calculated collision rate coefficient (see Table 1). Also indicated are the observed reaction channels and the electronic configurations of the atomic cations. The reactions of Tc^+ and Po^+ were not investigated. The numbers in parentheses indicate the number of sequential reactions of the same type. Trace amounts ($\leq$12%) of MCH_2^+ observed to be formed in the reactions of Os^+, Ir^+, Pt^+, and Au^+ have not been included since these may be formed from excited M^+.

ions investigated since the ionization energy of CH_3F is quite high, $IE(CH_3F) = 12.47 \pm 0.02$ eV.[25] Hydrogen atom transfer to produce $MH^+ + CH_2F$ is also endothermic because of the relatively low hydrogen atom affinities of M^+, $HA(M^+)$. Known values for $HA(M^+)$ are <66 kcal mol^{-1} for the atomic cations investigated here,[26−28] while $D(CH_2F-H) = 103 \pm 3$ kcal mol^{-1}.[25]

A total of 19 of the 46 reactions investigated exhibit one or two *bimolecular* channels. The remaining 27 reactions were relatively slow. A total of 25 of these (Mn^+, Fe^+, Co^+, Ni^+, Cu^+, Zn^+, Ga^+, Rb^+, Mo^+, Ru^+, Rh^+, Pd^+, Ag^+, Cd^+, In^+, Sn^+, Sb^+, Te^+, Cs^+, W^+, Re^+, Hg^+, Tl^+, Pb^+, Bi^+) were observed to proceed by addition, channel 1a, which is expected to proceed in a *termolecular* fashion, while the remaining 2 (K^+ and Se^+) showed no products at all in the flow regime investigated. The predominant addition reactions with Cr^+ and Au^+ were seen to compete with minor bimolecular reactions, and these could be attributed to excited states. Minor addition was observed to compete with major bimolecular channels in the reactions of As^+, Sr^+, and W^+. Finally, minor HF elimination, channel 1c, was observed to compete with H_2 elimination, channel 1d, in the reactions of Os^+, Ir^+, and Pt^+. Again, the minor channels could be attributed to excited states.

Figure 1 displays the data in Table 1 on a periodic table (excluding the minor competing channels attributed to excited states) and shows the trends in overall reaction efficiencies and product distributions across this table for the reactions of all 46 cations with CH_3F. It is immediately obvious from a quick glance at this table that the early-transition-metal cations exhibit a much more active chemistry than the late-transition-metal cations and that there are also periodic features in the chemical activity and reaction efficiency that maximize with Ti^+, As^+, Y^+, Hf^+, and Pt^+.

Fourth-Period Atomic Cations. With some important exceptions, the major *primary* reaction channel observed with fourth-period cations was either F atom transfer (with the early-transition-metal cations and Ge^+) or addition (with the late-transition-metal cations). The reaction of $As^+(p^2)$ proceeds primarily (97%) by HF elimination to establish $AsCH_2^+$ and only in minor amounts (3%) by addition (see Figure 2). The observation of an early rapid rise in the production of small amounts of CH_2F^+ (by hydride transfer, channel 1e) in the experiments with Cr^+ provided an indication of trace amounts (ca. 2%) of excited Cr^+ in the initial Cr^+ cation population (our previous calculations indicate that only 80% of the Cr^+ ions produced within the ICP are in the electronic ground state).[10] $K^+(s^0)$ and $Se^+(p^3)$ were observed to be nonreactive, $k < 1 \times 10^{-13}$ cm^3 molecule^{-1} s^{-1}. The FT-ICR reaction efficiencies previously reported by Harvey et al.[3] for F atom transfer from CH_3F to Ca^+ (0.08), Sc^+ (0.47), Ti^+ (0.40), and V^+ (0.11) generally are in agreement, within experimental error, with our values of 0.12, 0.50, 0.59, and 0.079, respectively.

Secondary and *tertiary* fluoride formation according to reactions 2 and 3, respectively, were observed with the early-transition-metal ions.

$$MF^+ + CH_3F \rightarrow MF_2^+ + CH_3 \ (M = Sc, Ti, \text{and } V) \quad (2a)$$

$$\rightarrow MF_2 + CH_3^+ \ (M = Ti) \quad (2b)$$

$$MF_2^+ + CH_3F \rightarrow MF_3^+ + CH_3 \ (M = Sc \text{ and } Ti) \quad (3a)$$

$$\rightarrow MF_3 + CH_3^+ \ (M = Ti) \quad (3b)$$

A hydride transfer reaction between MF_2^+ and CH_3F to give CH_2F^+ and presumably MF_2H according to reaction 4 was observed with M = Sc and Ti.

$$MF_2^+ + CH_3F \rightarrow CH_2F^+ + MF_2H \quad (4)$$

Secondary and higher order CH_3F addition was observed with $M^+ = Mn^+$, Fe^+, Co^+, Cu^+, Zn^+, and Ga^+ ($n = 1$) and Ni^+ and Cr^+ ($n = 1-3$), $MF^+ = CaF^+$ and GeF^+ ($n = 0-1$) and

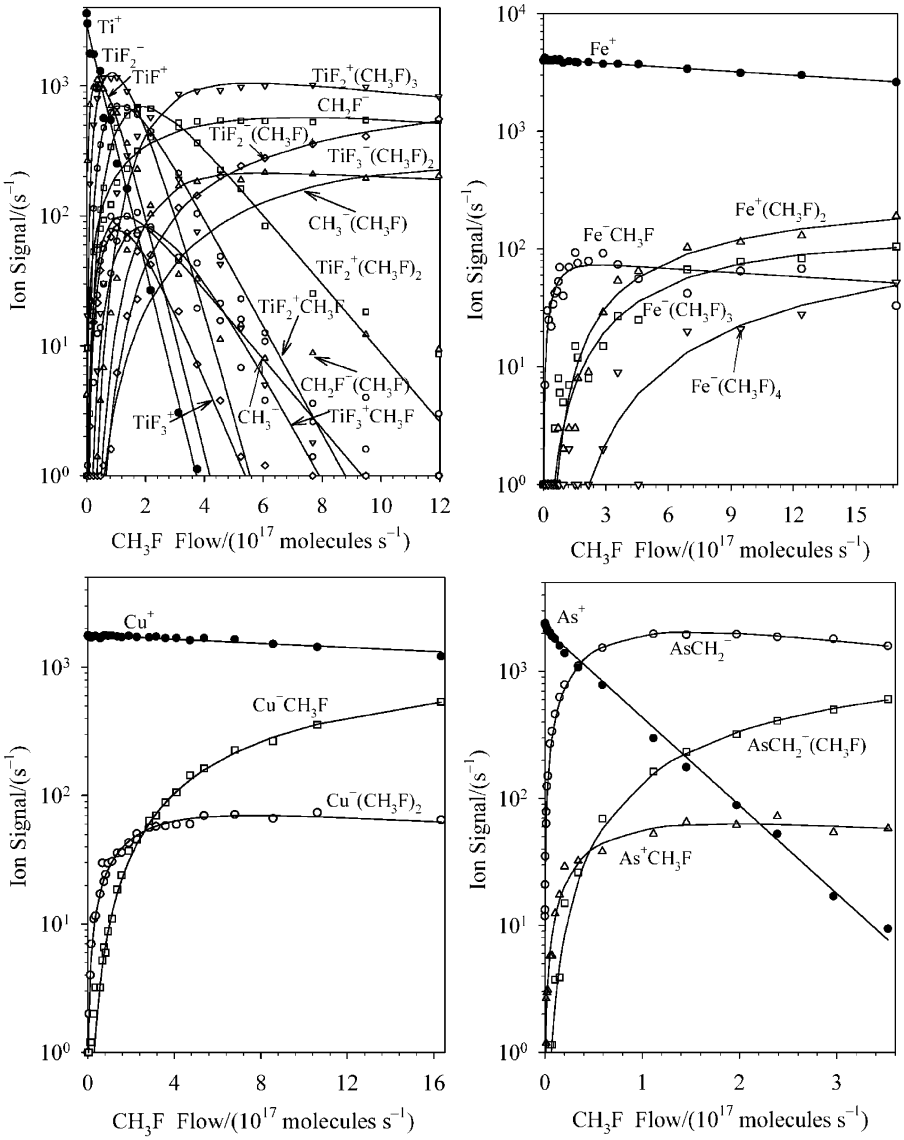

Figure 2. Composite of ICP/SIFT results for the reactions of the fourth-period atomic cations Ti^+, Fe^+, Cu^+, and As^+ with CH_3F in helium buffer gas at 0.35 ± 0.01 Torr and 295 ± 2 K.

VF^+ ($n = 0-4$), $MF_2^+ = ScF_2^+$, TiF_2^+, and VF_2^+ ($n = 0-3$), and $MF_3^+ = ScF3^+$ and TiF_3^+ ($n = 0-2$) cations according to reactions 5−8.

$$M^+(CH_3F)_n + CH_3F \rightarrow M^+(CH_3F)_{n+1} \quad (5)$$

$$MF^+(CH_3F)_n + CH_3F \rightarrow MF^+(CH_3F)_{n+1} \quad (6)$$

$$MF_2^+(CH_3F)_n + CH_3F \rightarrow MF_2^+(CH_3F)_{n+1} \quad (7)$$

$$MF_3^+(CH_3F)_n + CH_3F \rightarrow MF_3^+(CH_3F)_{n+1} \quad (8)$$

All of these addition reactions are expected to be termolecular, with He buffer gas atoms acting as the stabilizing third body. Figure 2 provides data for the chemistry of Ti^+, Fe^+, Cu^+, and As^+ that exhibit the occurrence of each of the reactions 2−8 above.

Fifth-Period Atomic Cations. Without exception, either F atom transfer or CH_3F addition was the observed *primary* product channel with atomic cations in the fifth period. F atom transfer was observed for four atomic cations, Sr^+, Y^+, Zr^+, and Nb^+. The FT-ICR reaction efficiency previously reported by Harvey et al.[3] for F atom transfer from CH_3F to Y^+ (0.86) is in exact agreement with our result of 0.86. CH_3F addition was observed for the remaining 11 atomic ions in this period (excluding Tc^+).

Secondary and higher order fluoride formation according to reaction 9 was observed for the early-transition-metal ions of $M^+ = Y^+$, Zr^+, and Nb^+ with n up to 1, 2, and 4, respectively.

$$MF_n^+ + CH_3F \rightarrow MF_{n+1}^+ + CH_3 \quad (9)$$

Secondary and higher order CH_3F addition was observed for $M^+ = Cd^+$, Sn^+, and Sb^+ ($n = 1$), Ru^+, Rh^+, Pd^+, and Ag^+ ($n = 1-2$), and Mo^+ ($n = 1-3$) and YF_2^+ ($n = 0-2$) cations according to reactions 5−7 and NbF_4^+ ($n = 0-1$) according to reaction 10.

$$MF_4^+(CH_3F)_n + CH_3F \rightarrow MF_4^+(CH_3F)_{n+1} \quad (10)$$

Again, all of these addition reactions are expected to be termolecular, with He buffer gas atoms acting as the stabilizing third body and are seen to operate with Y^+, Rh^+, Pd^+, and Sb^+

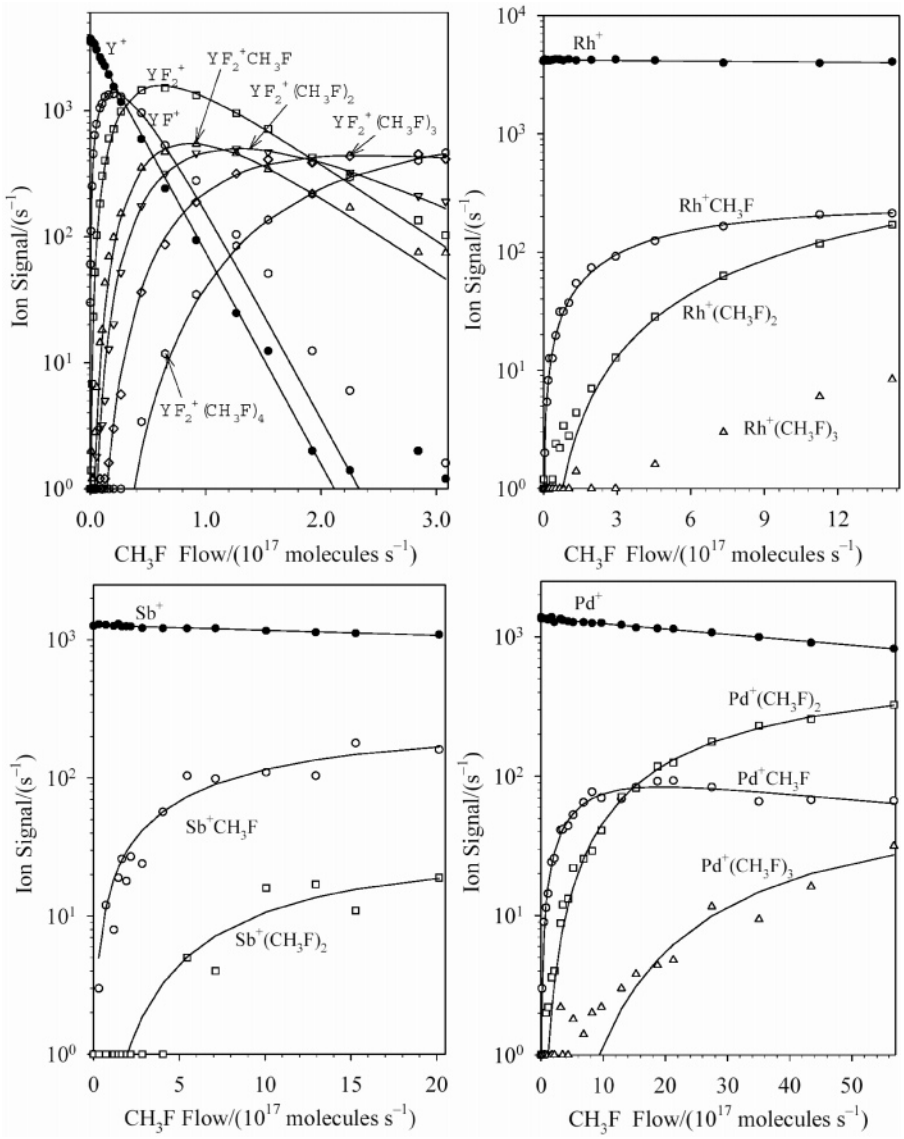

Figure 3. Composite of ICP/SIFT results for the reactions of the fifth-period atomic cations Y^+, Rh^+, Pd^+, and Sb^+ with CH_3F in helium buffer gas at 0.35 ± 0.01 Torr and 295 ± 2 K.

in Figure 3, which provides experimental data obtained for the chemistry of these cations.

We can report here that our results for the reactions of Sr^+ and Rb^+ parallel those obtained in a dynamic reaction cell study of the $^{87}Rb^+/^{87}Sr^+$ isobaric interference.[15] These two cations react quite differently and with different rates: Sr^+ reacts only by F atom transfer ($k = 1.4 \times 10^{-11}$ cm^3 molecule^{-1} s^{-1}), and Rb^+ reacts only by CH_3F addition ($k = 1.3 \times 10^{-12}$ cm^3 molecule^{-1} s^{-1} in He at 0.35 Torr). It is precisely these attributes that make CH_3F so attractive for the chemical resolution of this isobaric interference.

Sixth-Period Atomic Cations. Dehydrogenation is a striking feature of the *primary* chemistry exhibited by some of the sixth-period atomic cations. In addition to F atom transfer (observed with Ba^+, La^+, Hf^+, and Ta^+) and CH_3F addition (observed with Cs^+, W^+, Re^+, Au^+, Hg^+, Tl^+, Pb^+, and Bi^+), dehydrogenation, channel 1d, was observed with Os^+ (>99%), Ir^+ (97%), and Pt^+ (95%). Some HF elimination to form MCH_2^+ cations was observed to compete in the reactions with $M^+ = Os^+$ (2%), Ir^+ (3%), Pt^+ (5%), and Au^+ (12%). The source of these minor product ions is not unambiguous; they may arise from either ground-state or excited M^+ cations given the amounts of excited M^+ that have been estimated to be formed in the ICP for Ir^+, Pt^+, and Au^+ (Os^+ could not be estimated).[10] We do have previous evidence for the presence of excited Pt^+ in the reaction region.[10]

Secondary and higher order fluoride formation was observed with the transition-metal ions $M^+ = Hf^+$ and Ta^+. Higher order fluoridation according to reaction 9 was observed with $M^+ = Hf^+$ (n up to 2) and Ta^+ (n up to 4). Secondary and higher order CH_3F addition was observed for $M^+ = Au^+$ and Hg^+ ($n = 1$), Re^+ and Os^+ ($n = 1-2$), and W^+ ($n = 1-3$), $MF^+ = BaF^+$ ($n = 1-2$), $MF_3^+ = HfF_3^+$ ($n = 0-1$), and $MF_4^+ = TaF_4^+$ ($n = 0-1$) according to reactions 5, 6, 8, and 10. All of these addition reactions are expected to be termolecular, with He buffer gas atoms acting as the stabilizing third body. The secondary and higher order chemistry with Hf^+, Ta^+, Ir^+, and Au^+ is evident in Figure 4.

Efficiency and Mechanism of Fluorine Atom Transfer. F atom transfer was observed with group 2 atomic ions (Ca^+, Sr^+, Ba^+), with group 3 (Sc^+, Y^+, La^+), group 4 (Ti^+, Zr^+, Hf^+), and group 5 (V^+, Nb^+, Ta^+) transition-metal cations, and with Ge^+. The rate coefficients measured for F atom transfer are in the range from 1.4×10^{-11} cm^3 molecule^{-1} s^{-1} (for Sr^+) to 1.5×10^{-9} cm^3 molecule^{-1} s^{-1} (for Y^+).

There is good agreement between our ICP/SIFT results and

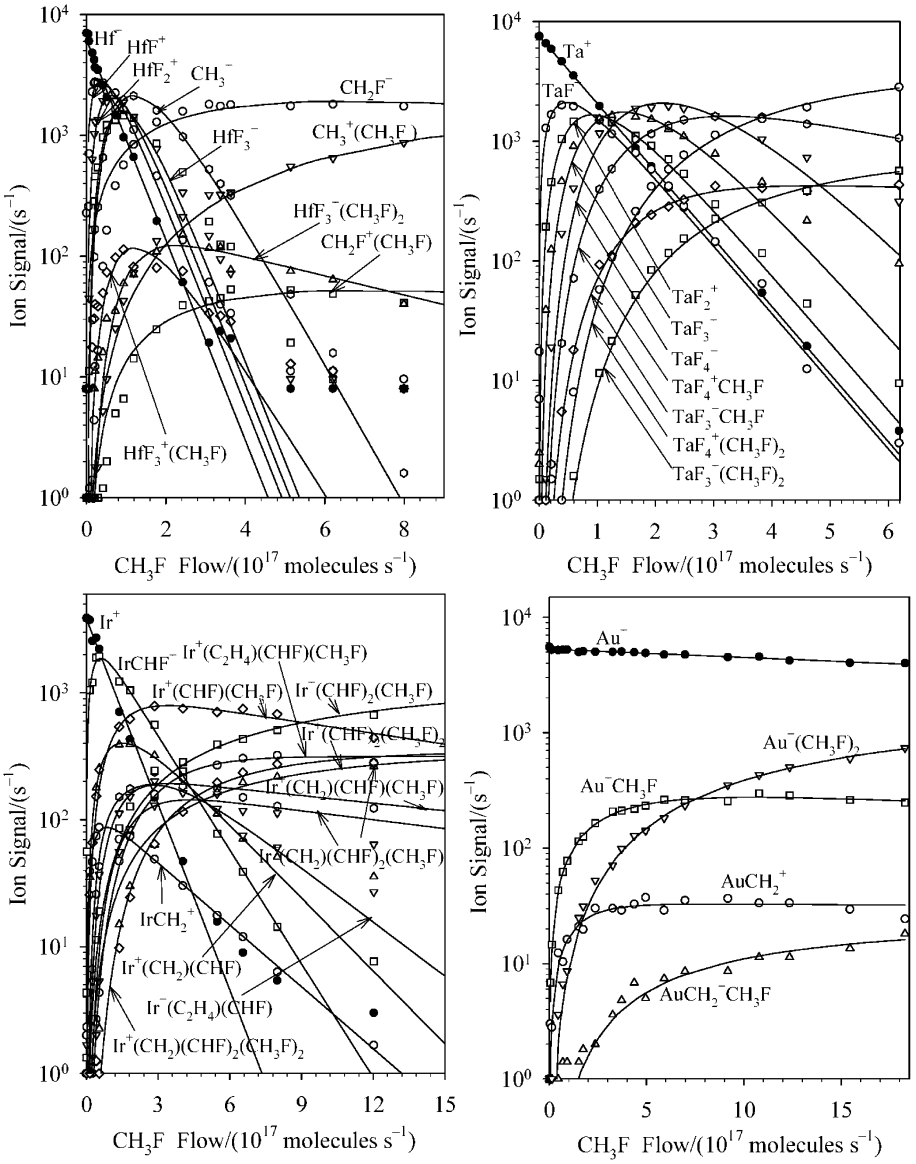

Figure 4. Composite of ICP/SIFT results for the reactions of the sixth-period atomic cations Hf^+, Ta^+, Ir^+, and Au^+ with CH_3F in helium buffer gas at 0.35 ± 0.01 Torr and 295 ± 2 K.

those reported in a previous, albeit more limited, FT-ICR study of reactions of M^+ ions with CH_3F.[4] Fluorine atom transfer from CH_3F was observed using FT-ICR for Ca^+, Sc^+, Ti^+, V^+, and Y^+ with efficiencies of 0.08, 0.47, 0.40, 0.11, and 0.86, respectively, which agree, within experimental uncertainty, with our values of 0.12, 0.49, 0.59, 0.079, and 0.77, respectively. The earlier ICR value for Ti^+ of 0.055 ($k = 1.2 \times 10^{-10}$ cm^3 molecule^{-1} s^{-1})[2] is about 10 times smaller than our value of 0.59 ($k = 1.3 \times 10^{-9}$ cm^3 molecule^{-1} s^{-1}). The precise origin of this discrepancy is not clear, but these early ICR results may have been influenced by a poor pressure calibration.

The F atom transfer channel 1b is exothermic if $D(M^+-F) > D(CH_3-F) = 113 \pm 1$ kcal mol^{-1}.[25] F atom affinities available for M^+ cations from either experiment or theory are listed in Table 2. These values indicate that F atom transfer is exothermic with Ca^+, Sc^+, Ti^+, Sr^+, and La^+ and endothermic with Cr^+, Fe^+, Ni^+, Cu^+, and Au^+. Secondary F atom transfer to ScF^+ is also exothermic. Our kinetic results indicate the occurrence of exclusive F atom transfer for all the exothermic reactions and CH_3F adduct formation with all the endothermic reactions. Therefore, the occurrence of F atom transfer appears to be thermodynamically controlled (see Figure 5), although

TABLE 2: F atom Affinities (kcal mol^{-1}), FA(M^+) = $D_T(M^+-F)$, for Some Atomic Cations

M^+	FA(M^+)	T/K	ref
Ca^+	131.0	0	29
	133.2 ± 2	298	30, 31
Sc^+	150.2	298	32
ScF^+	123.2	298	32
Ti^+	≥109	298	33
	118 ± 9	298	2
Cr^+	73	0	34
	71.5 ± 7.3	298	35
Fe^+	100.9	0	36
	92.5 ± 7.5	298	36
Co^+	91.9	0	37
Ni^+	≤109	298	38
Cu^+	76.2	0	39
Sr^+	131.7	0	29
La^+	174.9	0	40
Au^+	18	0	41
Tl^+	3.7	298	42
	0.5	0	43

Figure 1 shows a periodic variation in efficiency for F atom transfer observed with the early-transition-metal cations. On this basis we can predict the F atom affinities of V^+, Ge^+, Y^+, Zr^+,

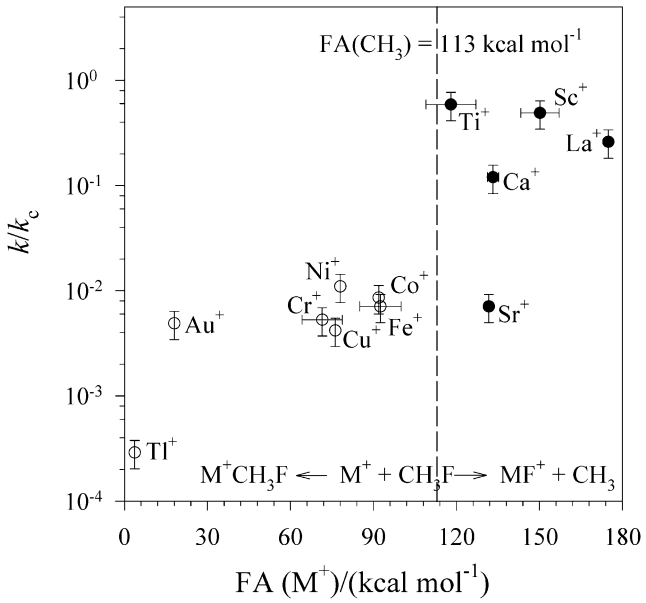

Figure 5. Dependence of the reaction efficiency, k/k_c, on the F atom affinity, FA, of the cation. k represents the measured reaction rate coefficient, and k_c is the calculated collision rate coefficient (see Table 1). Reactions on the right of the dashed line are exothermic for F atom transfer, while those on the left are endothermic. Solid circles indicate the observation of F atom transfer, while open circles indicate the observation of CH_3F addition.

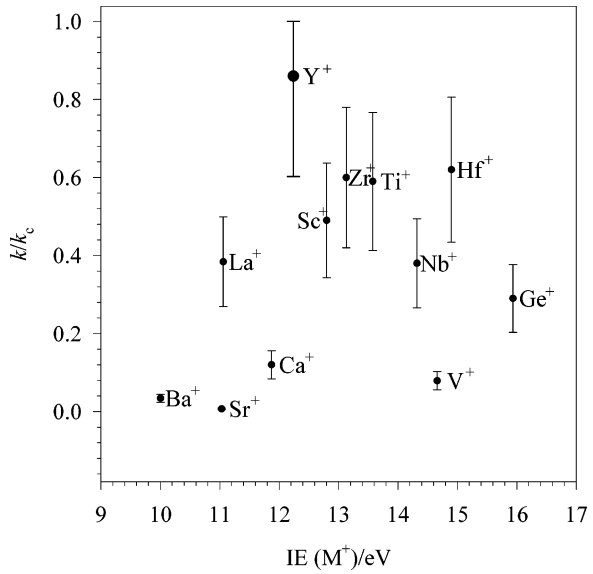

Figure 6. Variation in the efficiency, k/k_c, of F atom transfer from CH_3F to atomic cations with the second ionization energy of M, IE-(M^+). An uncertainty of 30% is assigned to the experimental value of k/k_c. Ionization energies are taken from ref 45.

Nb^+, Ba^+, Hf^+, and Ta^+, all of which were observed to react with CH_3F exclusively by F atom transfer, also to be $>113 \pm 1$ kcal mol^{-1}, and those of Mn^+, Co^+, Zn^+, Ga^+, Rb^+, Mo^+, Ru^+, Rh^+, Pd^+, Ag^+, Cd^+, In^+, Sn^+, Sb^+, Te^+, Cs^+, W^+, Re^+, Hg^+, Tl^+, Pb^+, and Bi^+, all of which were observed to react exclusively by CH_3F adduct formation, to be $<113 \pm 1$ kcal mol^{-1}.

Figure 5 shows the variation of reaction efficiency with available fluorine atom affinities, FA(M^+). The M^+ cations for which F atom transfer is endothermic react by CH_3F addition. The reaction efficiency is seen to be high for the transition-metal ions $Ti^+(^4F)$ and $Sc^+(^3D)$, but the exothermic F atom transfer reactions with the alkaline-earth (^2S) cation Ca^+, and especially Sr^+, proceed with low efficiency (as do those with $Ba^+(^2S)$ for which the fluorine atom affinity is not known). Our previous results with O atom transfer reactions of M^+ with N_2O suggest that low efficiencies for exothermic atom transfer can arise from intrinsic kinetic barriers or curve crossings that are required for the change in spin multiplicity that may be necessary for the overall spin to be conserved.[1] The low reactivity of Ca^+ has been previously addressed with ab initio computational studies of the potential energy surface for the reaction of Ca^+ with CH_3F for which the experimental reaction efficiency suggests a small kinetic barrier lying in the vicinity of the energy of the entrance channel.[3] Density-functional calculations led to an underestimate of the reaction barrier, whereas ACPF and CCSD(T) calculations with large basis sets provided good agreement with experiment.[3] Further analysis of the curve-crossing behavior of the potential energy surface in the vicinity of the transition state using valence bond theory indicated a tightly bonded transition state in which an electron is transferred from calcium to CH_3F before the ensuing bonding of Ca^{2+} with a fluoride anion (a so-called "structured harpoon" mechanism)[3] similar to the harpoon-like mechanism suggested previously for reactions of lanthanide atomic cations with CH_3F.[4] The correlation of reaction efficiencies with IE(M^+) expected from such a mechanistic scheme is not supported by our measurements (see Figure 6) as was also the case in our previous systematic study of F atom transfer reactions of lanthanide cations with CH_3F.[16] Thus, our measurements of F atom transfer reactions of atomic cations with CH_3F indicate a preference for the insertion/elimination mechanism commonly accepted for bond-activation reactions with other related molecules such as CH_4.[44]

HF and H_2 Elimination. HF elimination was observed as the major reaction channel with As^+ (97%) and a minor competing channel in the reaction with Os^+ (2%), Ir^+ (3%), Pt^+ (5%), and Au^+ (12%). As far as we are aware, there has been no previous report of such a reaction channel for reactions of atomic cations with CH_3F at 300 K. However, hydrogen halide elimination has been observed previously for the reactions of Au^+ with CH_3X (X = Cl, Br, and I)[45,46] and for the reactions of $Cu^+(^1S, ^3D)$ and $Au^+(^1S, ^3D)$ with CH_3Br.[47]

The high reactivity of As^+ is remarkable, especially in comparison with the much lower ($\geq$100 times) and different reactivity of Sb^+ and Bi^+, even though all three cations have a $d^{10}s^2p^2$ electronic configuration with two p electrons available for bonding. We do not have thermodynamic information on the $:CH_2$ affinities of these three cations, although we do know that the O atom affinity decreases down this column on the periodic table. Therefore, As^+ is the cation with perhaps the highest $:CH_2$ affinity of these three atomic cations (it has the highest O atom affinity)[10] and so may well be the only atomic cation of these three for which $M^+{=}CH_2$ formation is exothermic (just as appears to be the case for $As^+{=}O$ formation in O atom transfer with N_2O).[10] Assuming that the observed HF elimination reaction with As^+ is exothermic, we can recommend that $D(As^+{-}CH_2) \geq D(HF{-}CH_2) = 87$ kcal mol^{-1}.[25]

The dominant reaction channel for the reactions of the triad Os^+ (98%), Ir^+ (97%), and Pt^+ (95%) with CH_3F is dehydrogenation to produce $MCHF^+$. This suggests that $D(M^+{-}CHF) \geq D(H_2{-}CHF) = 85 \pm 3$ kcal mol^{-1} for these three transition metals.[25] The dehydrogenation channel has not been observed previously in studies of metal ions with alkyl halides,[46,47] but has been reported for reactions of transition-metal ions with various alkanes.[49−51]

CH_3F Addition. Addition of CH_3F was observed exclusively (>99%) with the late-fourth-period cations from Mn^+ to Ga^+,

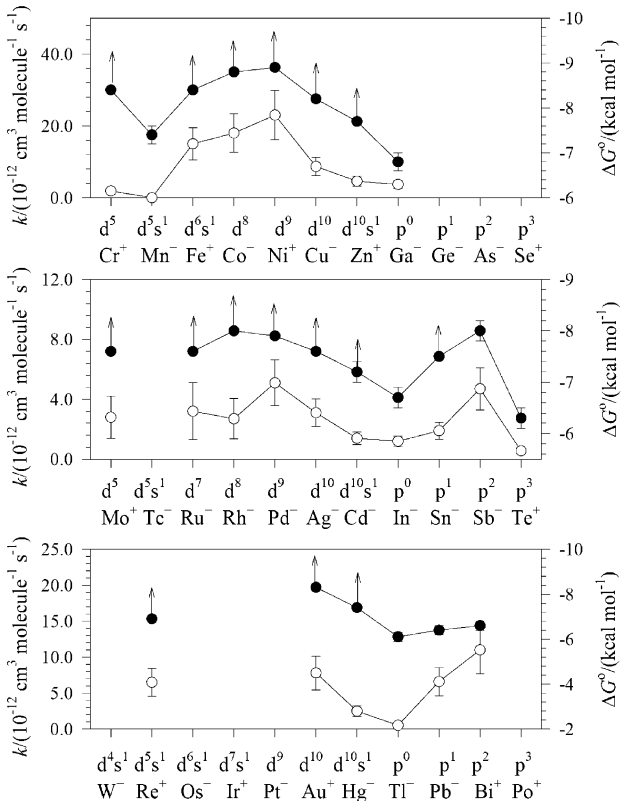

Figure 7. Variations observed in the effective bimolecular rate coefficient (open circles), *k*, and the standard free energy change (solid circles) for CH_3F addition with the electron configuration of the bare atomic cations.

the fifth-period cations from Ru^+ to Te^+, and the sixth-period cations from Hg^+ to Bi^+ as well as Re^+. All these addition reactions were observed to proceed with relatively small effective bimolecular rate coefficients, $\leq 7.8 \times 10^{-11}$ cm^3 molecule^{-1} s^{-1}, and are presumed to occur by collisional stabilization at 0.35 Torr of He, reaction 11,

$$M^+ + CH_3F + He \rightarrow M^+(CH_3F) + He \qquad (11)$$

rather than by radiative association (however, pressure-dependent studies were not performed). Figure 7 shows the variation in the magnitude of the effective bimolecular rate coefficients across the three periods of the periodic table for the CH_3F addition reactions that were investigated. No reactions or products were observed with K^+ (group 1), which has a rare-gas electron configuration, or with Se^+, which has a p^3 half-filled electron configuration. Failure to observe CH_3F addition with these two ions can be attributed to the weaker bonding with CH_3F expected from these electronic configurations. Weak bonding will decrease the rate of addition by decreasing the lifetime of the intermediate adduct ion and also may lead to adduct dissociation upon sampling. Indeed, the periodic trends in effective bimolecular rate coefficients apparent in Figure 7 are consistent with expected trends in the binding energies of the adduct ions. Since the degrees of freedom of the intermediate adduct ions are the same for this family of reactions, the relative lifetimes of the intermediates and therefore the effective bimolecular rate coefficients for addition will be sensitive *only to the binding energies*. We saw this recently for addition reactions of these same atomic ions with CO_2 and CS_2.[11,12] The bonding with these two molecules, as well as with CH_3F, is expected to be primarily electrostatic so that variations in binding energy should follow the trend in ion size and the trend

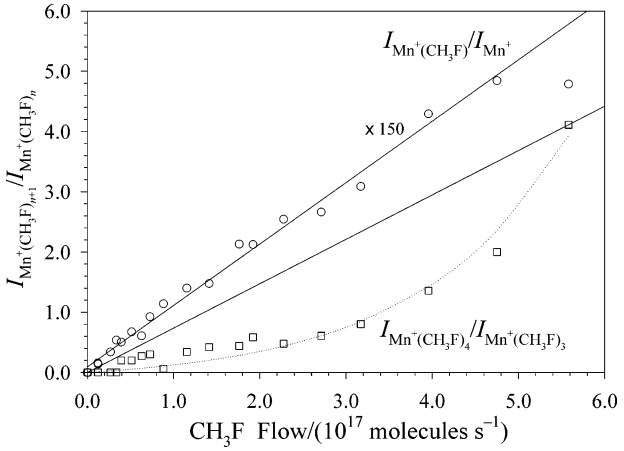

Figure 8. Ion signal ratio plots showing the observed variation in the ion signal ratios for $Mn^+(CH_3F)/Mn^+$ and $Mn^+(CH_3F)_4/Mn^+(CH_3F)_3$ with the flow of CH_3F. The first CH_3F addition exhibits equilibrium, while the fourth CH_3F addition does not but exhibits an approach to equilibrium (the straight line drawn through the last data point provides a lower limit to the equilibrium constant).

in repulsion between the metal d orbitals and the occupied orbitals of CH_3F. Therefore, minima in the binding energy in the fourth period should appear for $Mn^+(3d^54s^1)$ and $Ga^+(3d^{10}4s^24p^0)$ with which the repulsion is largest. The increase in M^+-CH_3F attraction due to decreasing size determines the trend in increasing bond energy observed just beyond Mn^+ and Ga^+. These minima give rise to the minima in the periodic variation in the effective bimolecular rate coefficient for CH_3F addition seen in Figure 7 and also the minima seen with In^+ in the fifth period and Tl^+ in the sixth period.

We also have explored the variation in the binding energy of the observed adduct ions by attempting to determine the standard free energies of addition from measurements of equilibrium constants. The variations in standard free energy should be similar to variations in the binding energy or enthalpy since large variations in the entropy change are not expected. A typical standard entropy change[52] for addition of a ligand to atomic ions of $-20(\pm 5)$ cal mol^{-1} K^{-1} would lead to $\Delta H^\circ = \Delta G^\circ - 6(\pm 1.5)$ kcal mol^{-1}.

Equilibrium analyses performed on the kinetic results indicate that equilibrium is attained in some of the CH_3F addition reactions. These analyses are based on plots of product-to-reactant ion signal ratios as a function of CH_3F flow. Equilibrium is achieved when this plot achieves linearity, viz., when $[M^+(CH_3F)_{n+1}]/[M^+(CH_3F)_n] = K[CH_3F]$. Some ion signal ratio plots were nicely linear, whereas others only approached linearity. The latter provide only lower limits to *K* (see Figure 8).

Higher Order F Atom Transfer. Two or more sequential F atom transfer reactions were observed with the early-transition-metal cations (groups 3−5). The number of sequential F atom transfer reactions increases across the periodic table from two to four, maximizing at four for the group 5 cations $Nb^+(d^4)$ and $Ta^+(d^3s^1)$. These results can be understood simply in terms of electron pairing, although $V^+(d^4)$, which was observed to add only two F atoms in succession, appears to be anomalous.

Table 4 lists the rate coefficients for primary and higher order F atom transfer that could be measured, and Figure 9 shows graphically how they vary with the number of F atoms transferred for reactions of CH_3F with group 3−5 atomic metal cations. With the exception of the reaction of VF^+, the rate coefficients for the second F atom transfer are all somewhat

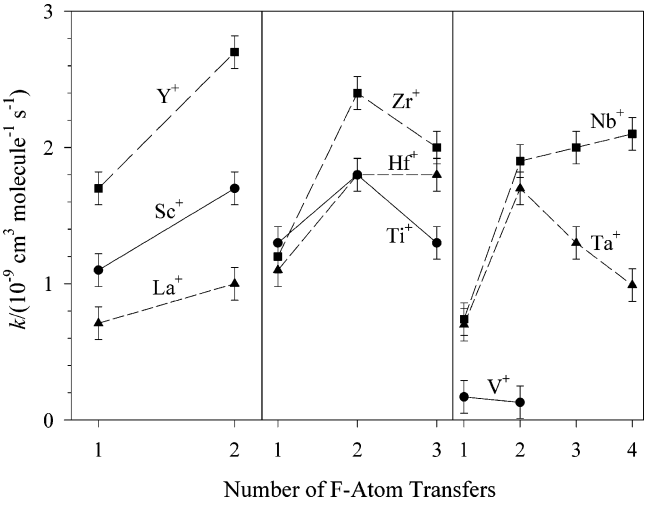

Figure 9. Observed variation of the rate coefficient with the number of F atoms transferred for reactions of CH_3F with group 3−5 atomic metal cations. The rate coefficients for the reactions with TiF_2^+, ZrF_2^+, and HfF_2^+ are the total rate coefficients for MF_3^+, CH_2F^+, and CH_3^+ formation. The rate coefficient for the reaction with VF^+ is the total rate coefficient for formation of VF_2^+ and $VF^+(CH_3F)$.

higher, but not more than 2.6 times, than that for the first F atom transfer.

MF_3^+ formation by reaction 2a was observed exclusively with NbF_2^+ and TaF_2^+ and competed with CH_2F^+, CH_3^+, and $MF_2^+(CH_3F)$ formation in the reactions with TiF_2^+, ZrF_2^+, and HfF_2^+. MF_4^+ formation was restricted to Nb and Ta; NbF_4^+ and TaF_4^+ reacted further with CH_3F by addition with effective bimolecular rate coefficients of $k = 6.4 \times 10^{-10}$ and 7.4×10^{-10} cm^3 molecule^{-1} s^{-1}, respectively (see Figure 4).

The internal energy distributions of the reacting MF_n^+ ($n > 0$) ions are not known since they are formed in exothermic reactions within the reaction region and may not be totally relaxed by collisions with the helium buffer gas atoms prior to their further reaction.

Higher Order CH_3F Addition. At least two CH_3F molecules were observed to add sequentially to the fourth-period cations Cr^+ (1.0), Mn^+ (1.1), Fe^+ (8.9), Co^+, Ni^+ (5.9), Cu^+ (3.3), Zn^+ (0.34), and Ga^+, the fifth-period cations Mo^+ (0.87), Ru^+ (0.89), Rh^+ (0.97), Pd^+ (0.90), Ag^+, Cd^+ (0.18), Sn^+ (0.19), and Sb^+, and the sixth-period cations W^+ (0.19), Re^+, and Hg^+, where the number in parentheses is the measured effective bimolecular rate coefficient for the second addition in units of 10^{-11} cm^3 molecule^{-1} s^{-1}. Most of these rate coefficients are up to 4 times higher, $k \geq 1.8 \times 10^{-12}$ cm^3 molecule^{-1} s^{-1}, than the primary ones, and this can be attributed to the increased number of degrees of freedom in the secondary reaction intermediate, which leads to longer intermediate lifetimes and so higher rates of collisional stabilization. Similar behavior also has been observed in our laboratory for other related systems.[7,53,54] Exceptions are seen for Cr^+ (1.1 > 1.0), Zn^+ (0.46 > 0.34), Sn^+ (0.19 = 0.19), and W^+ (0.95 > 0.19), and these may point to the influence of the relative binding energy of the adducts on the intermediate lifetime. It is not possible to be more definitive.

A large number of the higher order CH_3F addition reactions were also observed to approach and attain equilibrium under the flow tube conditions that were employed. Table 3 lists the absolute and limiting values for equilibrium constants that were measured for the addition of up to four molecules of CH_3F to various M^+ ions. Also included are the standard free energies of association derived from $\Delta G° = -RT \ln K$ at 295 ± 2 K. The standard free energies for CH_3F addition that are reported in Table 3 are generally unknown from previous measurements or calculations, as far as we are aware. There is not much to be discussed about trends in these data since many of the measured equilibrium constants simply are lower limits and the standard free energies derived from them are upper limits. In one case (Mn^+) there is a definite increase in $-\Delta G°$ for the addition of a second ligand and in another (Pd^+) a definite decrease in $-\Delta G°$ for the addition of a third ligand.

CH_3F addition was also observed with all of the metal mono- and multifluoride ions that were formed (see Table 1). For these ions, higher order chemistry was observed under our operating conditions involving multistep (up to four) sequential addition of CH_3F to their mono- or multifluoride cations.

Higher Order Hydride and Fluoride Transfer. Unexpected and unusual higher order reactions were observed with the group 4 transition-metal cations $Ti^+(d^2s^1)$, $Zr^+(d^2s^1)$, and $Hf^+(d^1s^2)$ upon a careful inspection of the product ratio plots. The third F atom transfer was observed to compete with hydride transfer, reaction 12a, and fluoride transfer, reaction 12b,

$$MF_2^+ + CH_3F \rightarrow CH_2F^+ + HMF_2 \quad (12a)$$

$$\rightarrow CH_3^+ + MF_3 \quad (12b)$$

to form neutral, almost fully oxidized metal halides. This chemistry initiated by Ti^+ is summarized in Scheme 1 for illustration, along with the extensive clustering with methyl fluoride that ensues. The early ICR study of Uppal and Staley indicated the occurrence of the reaction sequence leading to the formation of CH_2F^+ from Ti^+ via the formation of TiF^+ and TiF_2^+.[2]

Table 1 includes the tertiary products and their CH_3F adducts observed with Zr^+ and Hf^+. ZrF_2^+ did not seem to undergo reaction 12a.

Higher Order HF and H_2 Elimination. The observed higher order chemical reactions initiated by the sixth-period cation Ir^+, and to a lesser extent W^+ and Os^+, and expressed in reactions 13−17,

$$WCHF^+ + CH_3F \rightarrow W(CHF)_2^+ + H_2 \quad (13)$$

$$OsCHF^+/OsCH_2^+ + CH_3F \rightarrow Os(CH_2)(CHF)^+ + HF/H_2 \quad (14)$$

$$IrCHF^+ + CH_3F \rightarrow Ir(CHF)_2^+ + H_2 \quad (15)$$

$$IrCHF^+/IrCH_2^+ + CH_3F \rightarrow Ir(CH_2)(CHF)^+ + HF/H_2 \quad (16)$$

$$Ir(CH_2)(CHF)^+ + CH_3F \rightarrow Ir(CH_2)_2(CHF)^+ + HF \quad (17)$$

are a repetition of the primary hydrogen and hydrogen fluoride elimination reactions seen with these cations. The internal energy distributions of the reacting secondary and tertiary ions are not known since they are formed in exothermic reactions within the reaction region and may not be totally relaxed by collisions with the helium buffer gas atoms prior to their further reaction. None of this chemistry appears to have been reported previously.

Conclusions

The room-temperature reactions of atomic transition-metal and main-group cations with CH_3F exhibit a range of channels and efficiencies that show a periodic variation across the periodic

TABLE 3: Equilibrium Constants, *K* (Standard State = 1 atm), Measured for Formation of $M^+(CH_3F)_n$ Ions from Sequential CH_3F Addition to Atomic Cations at 295 ± 2 K[a]

	K (Δ*G*°)			
M^+	$M^+(CH_3F)$	$M^+(CH_3F)_2$	$M^+(CH_3F)_3$	$M^+(CH_3F)_4$
Cr^+	$\geq 1.3 \times 10^6$ (≤ -8.4)	1.3×10^7 (-9.7)		
Mn^+	1.3×10^5 (-8.3)	2.8×10^6 (-8.8)		
Fe^+	$\geq 1.3 \times 10^6$ (≤ -8.4)	$\geq 1.3 \times 10^7$ (≤ -9.7)	$\geq 6.0 \times 10^7$ (≤ -10.6)	1.5×10^6 (-8.4)
Co^+	$\geq 2.7 \times 10^6$ (≤ -8.8)	4.0×10^7 (-10.4)		
Ni^+	$\geq 3.7 \times 10^6$ (≤ -8.9)	$\geq 3.0 \times 10^7$ (≤ -10.2)	$\geq 1.2 \times 10^7$ (≤ -9.6)	1.4×10^5 (-7.0)
Cu^+	$\geq 1.2 \times 10^6$ (≤ -8.3)	3.8×10^7 (-10.3)		
Zn^+	$\geq 4.8 \times 10^5$ (≤ -7.7)	$\geq 3.2 \times 10^6$ (≤ -8.9)		
Ga^+	1.0×10^5 (-6.8)			
Rb^+	4.3×10^4 (-6.3)			
Mo^+	$\geq 4.0 \times 10^5$ (≤ -7.6)	1.0×10^7 (-9.5)		
Ru^+	$\geq 4.0 \times 10^5$ (≤ -7.6)	1.0×10^7 (-9.5)		
Rh^+	$\geq 7.5 \times 10^5$ (≤ -8.0)	4.2×10^6 (-9.0)		
Pd^+	$\geq 6.0 \times 10^5$ (≤ -7.9)	7.0×10^6 (-9.3)	1.4×10^5 (-7.0)	
Ag^+	$\geq 4.0 \times 10^5$ (≤ -7.6)			
Cd^+	$\geq 2.0 \times 10^5$ (≤ -7.2)	7.1×10^5 (-8.0)		
In^+	8.4×10^4 (-6.7)			
Sn^+	$\geq 2.9 \times 10^5$ (≤ -7.5)	6.0×10^5 (-7.9)		
Sb^+	7.3×10^5 (-8.0)			
Te^+	4.2×10^4 (-6.3)			
Cs^+	2.8×10^4 (-6.1)			
Re^+	$\geq 1.2 \times 10^5$ (≤ -6.9)			
Au^+	$\geq 1.3 \times 10^6$ (≤ -8.3)	1.0×10^7 (-9.6)		
Hg^+	$\geq 2.8 \times 10^5$ (≤ -7.4)			
Tl^+	3.2×10^4 (-6.1)			
Pb^+	4.9×10^4 (-6.4)			
Bi^+	6.5×10^4 (-6.6)			

[a] The standard free energy changes, $\Delta G°(\text{kcal mol}^{-1}) = -RT \ln K$, are given in parentheses and have an uncertainty estimated to be no more than 0.3 kcal mol^{-1}.

TABLE 4: Rate Coefficients (cm^3 molecule^{-1} s^{-1}) Measured for Sequential F Atom Transfer

	first	second	third	fourth
Sc^+	1.1×10^{-9}	1.7×10^{-9}		
Ti^+	1.3×10^{-9}	1.8×10^{-9}	1.3×10^{-9} [a]	
V^+	1.7×10^{-10}	1.3×10^{-10} [b]		
Y^+	1.7×10^{-9}	2.7×10^{-9}		
Zr^+	1.2×10^{-9}	2.4×10^{-9}	2.0×10^{-9} [a]	
Nb^+	7.4×10^{-10}	1.9×10^{-9}	2.0×10^{-9}	2.1×10^{-9}
La^+	7.1×10^{-10}	1.0×10^{-9}		
Hf^+	1.1×10^{-9}	1.8×10^{-9}	1.8×10^{-9} [a]	
Ta^+	7.0×10^{-10}	1.7×10^{-9}	1.3×10^{-9}	9.9×10^{-10}

[a] Total reaction rate coefficients for MF_3^+, CH_2F^+, CH_3^+, and $M^+(CH_3F)$ formation. [b] The branching ratio for $VF_2^+/VF^+(CH_3F)$ formation was determined to be 3/7.

table that maximizes with Ti^+, As^+, Y^+, Hf^+, and Pt^+. Primary reaction channels include F atom transfer, CH_3F addition, HF elimination, and H_2 elimination. The early-transition-metal cations exhibit a much more active chemistry than the late-transition-metal cations. F atom transfer appears to be thermodynamically controlled but exhibits a periodic variation in efficiency with the early-transition-metal cations that maximizes with Ti^+, Y^+, and Hf^+. Addition of CH_3F occurs exclusively (>99%) with the late-fourth-period cations from Mn^+ to Ga^+, the fifth-period cations from Ru^+ to Te^+, and the sixth-period cations from Hg^+ to Bi^+ as well as Re^+. Periodic trends in the effective bimolecular rate coefficient for CH_3F addition are consistent with expected trends in the electrostatic binding energies of the adduct ions and measured trends in the standard free energy of addition. HF elimination is the major reaction channel with As^+, while dehydrogenation dominates the reactions of W^+, Os^+, Ir^+, and Pt^+. Sequential F atom transfer occurs with the early-transition-metal cations, with the number of F atoms transferred increasing across the periodic table from two to four, maximizing at four for the group 5 cations $Nb^+(d^4)$ and $Ta^+(d^3s^1)$, and stopping at two with $V^+(d^4)$. Sequential CH_3F addition occurs with many atomic cations and all of the metal mono- and multifluoride cations that were formed.

SCHEME 1

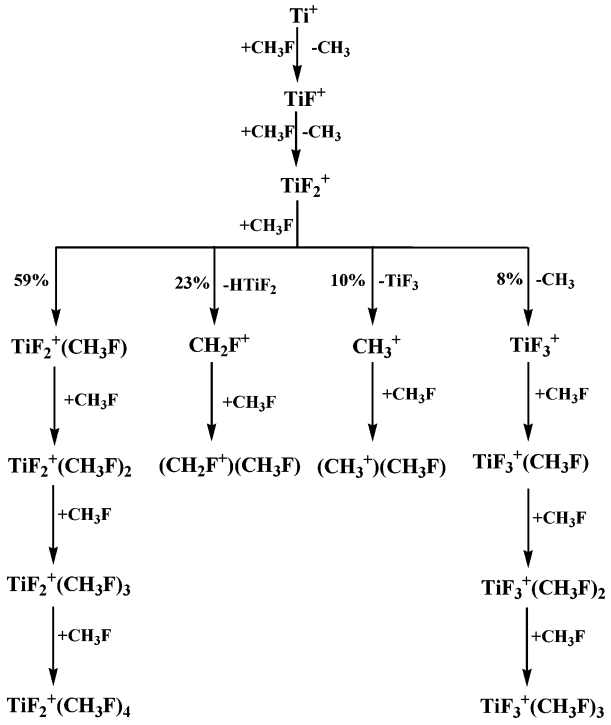

Acknowledgment. Continued financial support from the Natural Sciences and Engineering Research Council of Canada is greatly appreciated. Also, we acknowledge support from the National Research Council, the Natural Science and Engineering Research Council, and MDS SCIEX in the form of a Research Partnership grant. As holder of a Canada Research Chair in

Physical Chemistry, D.K.B. acknowledges the contributions of the Canada Research Chair Program to this research.

References and Notes

(1) Mazurek, U.; Schwarz, H. *Chem. Commun.* **2003**, 1321−1326.
(2) Uppal, J. S.; Staley, R. H. *J. Am. Chem. Soc.* **1980**, *102*, 4144−4149.
(3) Harvey, J. N.; Schröder, D.; Koch, W.; Danovich, D.; Shaik, S.; Schwarz, H. *Chem. Phys. Lett.* **1997**, *278*, 391−397.
(4) Cornehl, H. H.; Hornung, G.; Schwarz, H. *J. Am. Chem. Soc.* **1996**, *118*, 9960−9965.
(5) Koyanagi, G. K.; Caraiman, D.; Blagojevic, V.; Bohme, D. K. *J. Phys. Chem. A* **2002**, *106*, 4581−4590.
(6) Caraiman, D.; Bohme, D. K. *J. Phys. Chem. A* **2002**, *106*, 9705−9717.
(7) Caraiman, D.; Koyanagi, G. K.; Cunje, A.; Hopkinson, A. C.; Bohme, D. K. *Organometallics* **2002**, *21*, 4293−4296.
(8) Caraiman, D.; Koyanagi, G. K.; Bohme, D. K. *J. Phys. Chem. A* **2004**, *108*, 978−986.
(9) Koyanagi, G. K.; Bohme, D. K. *Int. J. Mass Spectrom.* **2003**, *227*, 563−575.
(10) Lavrov, V. V.; Blagojevic, V.; Koyanagi, G. K.; Orlova, G.; Bohme, D. K., *J. Phys. Chem. A* **2004**, *108*, 5610−5624.
(11) Koyanagi, G. K.; Bohme, D. K. *J. Phys. Chem. A* **2006**, *110*, 1232−1241.
(12) Cheng, P.; Koyanagi, G. K.; Bohme, D. K. *J. Phys. Chem. A* **2006**, *110*, 2718−2728.
(13) Mackay, G. I.; Vlachos, G. D.; Bohme, D. K.; Schiff, H. I. *Int. J. Mass Spectrom. Ion Phys.* **1980**, *36*, 259−270.
(14) Raksit, A. B.; Bohme, D. K. *Int. J. Mass Spectrom. Ion Processes* **1983**, *55*, 69−82.
(15) Moens, L. J.; Vanhaecke, F. F.; Bandura, D. R.; Baranov, V. I.; Tanner, S. D. *J. Anal. At. Spectrom.* **2001**, *16*, 991−994.
(16) Koyanagi, G. K.; Zhao, X.; Blagojevic, V.; Jarvis, M. J. Y.; Bohme, D. K. *Int. J. Mass Spectrom.* **2005**, *241*, 189−196.
(17) Koyanagi, G. K.; Lavrov, V. V.; Baranov, V.; Bandura, D.; Tanner, S.; McLaren, J. W.; Bohme, D. K. *Int. J. Mass Spectrom.* **2000**, *194*, L1−L5.
(18) Koyanagi, G. K.; Baranov, V. I.; Tanner, S. D.; Bohme, D. K. *J. Anal. At. Spectrom.* **2000**, *15*, 1207−1210.
(19) Moore, C. E. *Atomic Energy Levels as Derived from the Analyses of Optical Spectra*; NSRDS-NBS35; U.S. National Bureau of Standards: Washington, DC, 1971.
(20) Van Kleef, T. A. M.; Metsch, B. C. *Physica* **1978**, *C 95*, 251−265.
(21) Condon, E. U.; Shortley, G. H. *The Theory of Atomic Spectra*; Cambridge University Press: Cambridge, U.K., 1963.
(22) Su, T.; Chesnavich, W. J. *J. Chem. Phys.* **1982**, *76*, 5183−5185.
(23) Sutter, H.; Cole, R. H. *J. Chem. Phys.* **1970**, *52*, 132−139.
(24) Nelson, R. D., Jr.; Lide, D. R.; Maryott, A. A. *Selected Values of Electric Dipole Moments for Molecules in the Gas Phase*; NSRDS-NBS10; U.S. National Bureau of Standards: Washington, DC, 1967.
(25) Lias, S. G.; Bartmess, J. E.; Liebman, J. F.; Holmes, J. L.; Levin; D., R.; Mallard, W. G. *J. Phys. Chem. Ref. Data* **1988**, *17* (Suppl. 1), 1.
(26) Armentrout, P. B. *Int. J. Mass Spectrom.* **2003**, *227*, 289−302.
(27) Pettersson, L. G. M.; Bauschlicher, C. W., Jr.; Langhoff, S. R.; Partridge, H. *J. Chem. Phys.* **1987**, *87*, 481−492.
(28) Ohanessian, G.; Brusich, M. J.; Goddard, W. A., III. *J. Am. Chem. Soc.* **1990**, *112*, 7179−7189.
(29) Partridge, H.; Langhoff, S. R.; Bauschlicher, C. W., Jr. *J. Chem. Phys.* **1986**, *84*, 4489−4496.
(30) Chase, M. W.; Davies, C. A.; Downey, J. R.; Fruip, K. J.; McDonald, R. A.; Syverud, A. N. *J. Phys. Chem. Ref. Data* **1985**, *14* (Suppl. 1).
(31) Murphy, J. E.; Berg, J. M.; Merer, A. J.; Harris, N.; Field, R. W. *Phys. Rev. Lett.* **1990**, *65*, 1861.
(32) Jiao, C. Q.; Freiser, B. S. *J. Am. Chem. Soc.* **1993**, *115*, 6268−6276.
(33) Allison, J.; Ridge, D. P. *J. Am. Chem. Soc.* **1978**, *100*, 163−169.
(34) Harrison, J. F. *J. Phys. Chem.* **1986**, *90*, 3313−3319.
(35) Mazurek, U.; Schröder, D.; Schwarz, H. *Collect. Czech. Chem. Commun.* **1998**, *63*, 1498−1512.
(36) Schröder, D.; Hrusak, J.; Schwarz, H. *Helv. Chim. Acta* **1992**, *75*, 2215−2218.
(37) Chen, Q.; Freiser, B. S. *J. Phys. Chem. A* **1998**, *102*, 3343−3351.
(38) Allison, J.; Ridge, D. P. *J. Am. Chem. Soc.* **1979**, *101*, 4998−5009.
(39) Schwerdtfeger, P.; Boyd, P. D. W.; Bowmaker, G. A.; Aldridge, L. P. *Struct. Chem.* **1990**, *1*, 405−415.
(40) Zhang, D. J.; Zhang, C. Q.; Liu, C. B. *J. Organomet. Chem.* **2001**, *640*, 121−126.
(41) Schwerdtfeger, P.; McFeaters, J. S.; Liddell, M. J.; Hrusak, J.; Schwarz, H. *J. Chem. Phys.* **1995**, *103*, 245−252.
(42) *NIST Standard Reference Database 69*; National Institute of Standards: Gaithersburg, MD, 2003; http://webbook.nist.gov/chemistry/.
(43) Schroeder, D.; van Wuellen, C.; Schwarz, H.; Klapoetke, T. M. *Angew. Chem., Int. Ed.* **2005**, *44*, 4254−4257.
(44) Cornehl, H. H.; Heinemann, C.; Schröder, D.; Schwarz, H. *Organometallics* **1995**, *14*, 992−999.
(45) Lide, D. R. *CRC Handbook of Chemistry and Physics*, 85th ed.; CRC Press: Boca Raton, FL, 2005.
(46) Chowdhury, A. K.; Wilkins, C. L. *J. Am. Chem. Soc.* **1987**, *109*, 5336−5343.
(47) Brown, J. R.; Schwerdtfeger, P.; Schröder, D.; Schwarz, H. *J. Am. Soc. Mass Spectrom.* **2002**, *13*, 485−492.
(48) Taylor, W. S.; May, J. C.; Lasater, A. S. *J. Phys. Chem. A* **2003**, *107*, 2209−2215.
(49) Tolbert, M. A.; Mandich, M. L.; Halle, L. F.; Beauchamp, J. L. *J. Am. Chem. Soc.* **1986**, *108*, 5675−5683.
(50) Sievers, M. R.; Chen, Y. M.; Haynes, C. L.; Armentrout, P. B. *Int. J. Mass Spectrom.* **2000**, *195*, 149−170.
(51) Houriet, R.; Halle, L. F.; Beauchamp, J. L. *Organometallics* **1983**, *2*, 1818−1829.
(52) Kebarle, P. *Annu. Rev. Phys. Chem.* **1977**, *28*, 445−476.
(53) Baranov, V.; Bohme, D. K. *Int. J. Mass Spectrom.* **2001**, *210*, 303−310.
(54) Milburn, R. K.; Baranov, V.; Hopkinson, A. C.; Bohme, D. K. *J. Phys. Chem. A* **1999**, *103*, 6373−6382.